



1 **Expanding the simulation of East Asian Super Dust Storm: Physical** 2 **transport mechanism impacting the Western Pacific**

3 Steven Soon-Kai Kong ¹, Saginela Ravindra Babu ¹, Sheng-Hsiang Wang ¹, Stephen M. Griffith ²,
4 Jackson Hian-Wui Chang ^{1,3}, Ming-Tung Chuang ⁴, Guey-Rong Sheu ^{1,5,*}, Neng-Huei Lin ^{1,5,*}

5 ¹ Department of Atmospheric Sciences, National Central University, Taoyuan, 32001, Taiwan

6 ² Department of Atmospheric Sciences, National Taiwan University, Taipei, 10617, Taiwan

7 ³ Preparatory Center for Science and Technology, University Malaysia Sabah, Jalan UMS, 88400, Kota
8 Kinabalu, Sabah, Malaysia

9 ⁴ Research Center for Environmental Changes, Academia Sinica, Taipei, 11529, Taiwan

10 ⁵ Center for Environmental Monitoring and Technology, National Central University, Taoyuan, 32001,
11 Taiwan

12 *Correspondence to:* Neng-Huei Lin (nhlin@cc.ncu.edu.tw) and Guey-Rong Sheu
13 (grsheu@atm.ncu.edu.tw)

14 **Abstract.** Dust models are widely applied over the East Asian region for the simulation of dust
15 emission, transport and deposition. However, due to the uncertainties in estimates of dust flux, these
16 methods still lack the necessary precision to capture the complexity of transboundary dust events. This
17 study demonstrates an improvement in the Community Multiscale Air Quality (CMAQ) model dust
18 treatment during long-range transport of dust from northwest China to the South China Sea (SCS). To
19 accomplish this, we considered a super dust storm (SDS) event in March 2010, and evaluated the dust
20 scheme by including adjustments to the recent calibration (Dust_Refined_1) and bulk density
21 (Dust_Refined_2) refinements individually and in combination (Dust_Refined_3). The Dust_Refined_3
22 normalized mean bias of PM₁₀ was -30.73 % for the 2010 SDS event, which was lower compared to
23 Dust_Refined_1 (-41.34 %) and Dust_Refined_2 (-50.09 %). Indeed, the Dust_Refined_3 improved the
24 simulated AOD value during significant dust cases, for instance, in March 2005, March 2006 and April
25 2009. Dust_Refined_3 also showed more clearly that in March 2010, a 'double plume' (i.e., one plume
26 originated from the Taiwan Strait and the other from the Western Pacific) separated by the Central
27 Mountain Range (CMR) of Taiwan Island affected dust transport on Dongsha Island in the SCS. On 15-
28 21 April 2021, both CMAQ simulations and satellite data highlighted the influence of typhoon 'Surigae'
29 on dust transport to downwind Taiwan and the Western Pacific Ocean (WPO). The CMAQ



30 Dust_Refined_3 simulations further revealed a large fraction of dust aerosols were removed over WPO
31 due to typhoon ‘Surigae’. Hence, the model indicated near-zero dust particle concentration over the
32 WPO, which was significantly different from previous dust transport episodes over the Taiwan region.
33 Therefore, our study suggested an effective method to improve dust management of CMAQ under
34 unique topographical and meteorological conditions.

35 **1 Introduction**

36 Dust storms are a major source of dust aerosols and particles in outdoor air pollution, with significant
37 health, environmental and ecological impacts adjacent to and downwind of dust source regions,
38 especially in the East Asian region (Shao and Dong, 2006; Griffin and Kellogg, 2004; Yao et al., 2021).
39 Likewise, dust aerosols can significantly affect the Earth’s climate through direct and indirect
40 influences on the radiation balance of the atmosphere (Chen et al., 2017b; Huang et al., 2014; Dong et
41 al., 2019). The Gobi Desert (GD) in northern China and Mongolia, and the Taklamakan Desert (TD) in
42 western China are dust storm hotspot regions in East Asia. Several studies have reported on the impacts
43 of this East Asian Dust (EAD), particularly the effects during springtime on air quality and air pollution
44 over source regions (e.g. northern China) and over downwind regions such as Korea, Japan, and Taiwan
45 (Bian et al., 2011; Han et al., 2012; Guo et al., 2017; Jing et al., 2017; Dong et al., 2016; Jiang et al.,
46 2018; Kong et al., 2021, 2022; Tan et al., 2017; Uno et al., 2017). Fugitive dust can be dispersed over
47 thousands of miles; thus, regional and large-scale meteorological conditions play a crucial role in the
48 transport of these dust particles during dust storms.

49 A series of dust storms (15 March; 27 March; and 15 April) occurred over the Gobi Desert area
50 in the spring of 2021 including one of the largest dust storms in the past decade (15 March; “3.15” dust
51 storm hereafter). This severe dust storm turned the sky into sepia over Beijing (Sullivan, 2021), with
52 maximum PM₁₀ concentrations reaching up to 7,400 $\mu\text{g m}^{-3}$. A few studies investigated the origin,
53 transport processes, and impact of the “3.15” dust storm on air quality by multi-source observations and
54 numerical modeling (Liang et al., 2022; Gui et al., 2022; Jin et al., 2022; He et al., 2022). Gui et al.
55 (2022) reported the detailed spatial, temporal, and vertical evolution of the “3.15” dust storm and 27



56 March (“3.27” dust storm) events by utilizing satellite dust optical depths, lidar dust extinction profiles,
57 visibility measurements, and RGB Himawari imagery. Further, Jin et al. (2022), described the dust
58 sources, aerosol optical, microphysical, and radiative properties, and meteorological drivers of the three
59 events in 2021 spring. Even though past studies of more mild dust storm events have shown impacts as
60 far afield as the Taiwan region (Kong et al., 2021, 2022), most of the studies regarding 2021 super dust
61 storm (SDS) events were focused on the impact and transport over China and eastern downwind parts
62 of Asia. None of the studies reported the transport of dust from these events to the South China Sea
63 (SCS), including Taiwan, and also chemical-transport modeling of these events was limited.

64 On the other hand, several numerical modeling studies have been conducted to simulate March
65 2010 SDS event (Bian et al., 2011; He et al., 2022; Li et al., 2011; Zhao et al., 2011; Lin et al., 2012a;
66 Park et al., 2012; Chow et al., 2014; Chen et al., 2017a). Fortuitously, this SDS event was also detected
67 (Wang et al., 2011; 2012) over Dongsha Island (i.e. Pratas Island, 20°42052" N, 116°43051" E) in the
68 northern SCS during the Dongsha Experiment (<http://aerosol.atm.ncu.edu.tw>), which as part of the 7-
69 SEAS (the Seven South East Asian Studies; <http://7-seas.gsfc.nasa.gov>, Lin, et al., 2013) project was
70 designed to investigate the weather-aerosol interaction over Southeast Asia. Although the SDS arrival at
71 Dongsha Island was only described based on ground measuring and satellite imagery (Wang et al., 2011;
72 2012), these studies showed the possibility of transporting dust aerosol from northwest China to the
73 SCS boundary layer. However, a detailed high-resolution numerical modeling system is needed to
74 clarify the movement of the SDS aerosols in the region.

75 In previous our studies (Kong et al., 2021, 2022), we simulated moderate-intensity dust events at
76 the surface and at higher altitudes over the Taiwan region by using the Weather Research and
77 Forecasting-Community Multiscale Air Quality (WRF-CMAQ) model. Recognizing the opportunity to
78 model SDS events impacting Taiwan and the SCS, in this study we utilized the WRF-CMAQ model
79 with the latest windblown dust treatment to characterize the transport mechanism of the SDS events
80 over these downwind regions. As the notable amount of atmospheric mineral received by SCS over the
81 past years, that influences the oceanic ecosystem, a more detailed investigation regarding long-range
82 transport of dust episodes over the region can be vital (Duce et al., 1991; Wang et al., 2012). The



83 present manuscript is organized as follows. The methodology of the WRF-CMAQ model setup and dust
84 treatment calibration are discussed in Section 2. The results and discussion are presented in Section 3.
85 Finally, the summary and conclusions obtained from the present study are summarized in Section 4.

86 **2. Data and Methodology**

87 **2.1 WRF-CMAQ model setup and dust treatment calibration**

88 CMAQ is a state-of-the-art air quality model developed by the United States Environmental Protection
89 Agency USEPA (Appel et al., 2013) that distinguishes 19 chemical species within the dust particles,
90 thus providing a detailed description of dust mineralogy (Dong et al., 2016). Heterogenous chemistry
91 between the gas and aerosol phase also occurs (e.g. mechanisms) and can affect the dust chemical
92 composition, thus the gas-phase module is also activated in the model. This work utilized WRFv3.9.1
93 for the meteorological field prediction, and CMAQ v5.3.3 to simulate the transport of SDS on 18-24
94 March 2010, and several well-known severe dust storms, for instance, on 17-19 March 2005, 18-20
95 March 2006, 25-27 April 2009 and 23-21 April 2021 (Wang et al., 2012; Jin et al., 2022). The modeling
96 domain was set up to cover East Asia (d01), including the Gobi Desert, with a resolution of 81 km and
97 nested towards Taiwan at a resolution of 27 km (d02), 9 km (d03a), and 3 km (d04a) (Fig. 1a). The
98 nesting of Dongsha Island with 9 km and 3 km resolution (d03b and d04b) was set up to specifically
99 capture the long-range transport over the SCS. The model consisted of 40 vertical layers, with 8 layers
100 below ~1 km altitude, 13 layers below ~3 km altitude, and 27 layers covering the upper layer to ~21 km.
101 The initial and lateral boundary conditions of the model were constructed using the NCEP FNL re-
102 analysis dataset on a $1^\circ \times 1^\circ$ grid. The data assimilation was conducted by grid-nudging in all domains.
103 The CB06 gas-phase chemical mechanism and AERO7 aerosol module model were implemented in
104 CMAQ for the present study.

105 Anthropogenic emission inventories in East Asia were obtained from the MICS-Asia (Model
106 Inter-Comparison Study for Asia) Phase III emission inventory (Li et al., 2017). Biogenic emissions for
107 Taiwan were prepared by the Biogenic Emission Inventory System version 3.09 (BEIS3, Vukovich and
108 Pierce, 1988), and for regions outside Taiwan by Model of Emissions of Gases and Aerosols from



109 Nature v2.1 (MEGAN, Guenther, et al., 2012). TEDS 9.0 (Taiwan Emission Database System, TWEPA,
110 2011; <https://erdb.epa.gov.tw/>) was used for domain 4 (d04a) covering the Taiwan region, for the years
111 2005, 2006, 2009 and 2010, and TEDS 10.0 (TWEPA, 2021; <https://erdb.epa.gov.tw/>) was used for the
112 year 2021. Since domain d04b was specifically downscaled to Dongsha Island, no anthropogenic
113 emissions were applied for the region.

114 Five simulation scenarios including Dust_Off, Dust_Default, Dust_Refined_1, Dust_Refined_2,
115 and Dust_Refined_3 are presented and described in Table 1. The inline dust treatment was not included
116 in Dust_Off. For Dust_Default, wind speed, soil texture, and surface roughness length were integrated
117 based on the scheme by Foroutan et al. (2017). The performance of Dust_Off and Dust_Default in
118 simulating a moderate dust episode was compared by Kong et al. (2021), but this comparison has not
119 been investigated for a Super Dust Storm. This comparison provides important information as CMAQ is
120 often run for air quality purposes but with only Dust_Off or Dust_Default; yet, dust influence in that
121 observation data would be underestimated if using these basic schemes, thus reporting this performance
122 could be useful to later studies. The latest dust treatment over East Asia proposed by Kong et al. (2021)
123 was implemented in the Dust_Refined_1 scenario, which reduced the soil moisture at the surface and
124 revised the source-dependent species profile. The bulk soil density (ρ_b) should be revised to represent
125 the real soil type in China, which is represented by Dust_Refined_2 (Liu et al., 2021). As the default
126 bulk soil density (ρ_b) is set to $1,000 \text{ kg m}^{-3}$ in CMAQ for all soil types, the soil condition in China is not
127 specifically represented in the Dust_Default and Refined_1 scenario. Hence, the ρ_b of sand, loam,
128 sandy clay loam, and clay were revised as 1,550, 1,350, 1,450, and $1,300 \text{ kg m}^{-3}$, respectively, for
129 Dust_Refined_2 (Yu et al., 2015; Liu et al., 2021). Finally, Dust_Refined_3 combined the
130 Dust_Refined_1 and Dust_Refined_2 schemes.

131 2.2 Measurements at the downwind sites

132 The Dongsha Experiment included multiple platforms of instruments such as the
133 NASA/GSFC/COMMIT (Chemical, Optical, and Microphysical Measurements of In-situ Troposphere;
134 <http://smartlabs.gsfc.nasa.gov>) mobile observatory, the Taiwan Environmental Protection
135 Administration (TEPA) mobile facility, and a lidar system (EZ-Lidar; Leosphere Co.), of which detailed



136 information can be found in the literature (Wang et al., 2011). Briefly, continuous PM_{10} and $PM_{2.5}$ mass
137 concentrations were measured by a Tapered Element Oscillating Microbalance (TEOM; Model 1400 ab;
138 R&P Co.), which draws in air to a sample filter and changes the oscillation frequency of a calibrated
139 tapered element. This change in frequency is then converted to a particle mass based on the restoring
140 force constant of the tapered element. Moreover, a VAISALA WXT520 meteorological sensor was
141 specifically set up at Dongsha for the field campaign. It was used to measure weather conditions near
142 the surface, such as horizontal wind speed, wind direction, and precipitation. The dataset from Dongsha
143 Experiment was used to validate the CMAQ model precision during the dust storm event in March 2010.
144 In addition, the hourly PM_{10} concentration datasets from the Cape Fuguei, Wanli, Pingzhen, Hsinchu,
145 Xitun, Xinying, Zuoying, and Daliao sampling sites in Taiwan were obtained from the website of the
146 Taiwan Environmental Protection Agency (<https://data.epa.gov.tw/>).

147 **2.3 Reanalysis products and satellite measurements**

148 The Modern Era Retrospective-analysis for Research and Application version 2 (MERRA-2, Gelaro et
149 al., 2017) reanalysis data were used in this study to demonstrate the spatiotemporal distribution of dust
150 and compare it with the air quality model, irrespective of the cloud cover. MERRA-2 is a NASA
151 reanalysis ($0.5^\circ \times 0.625^\circ$ resolution) utilizing Goddard Earth Observing System Data Assimilation
152 System Version 5 (GEOS-5) and assimilates remotely sensed data. Besides, the level-3 MODIS AOD at
153 550 nm (MYD08) were used. The daily MODIS data was obtained from the AQUA platform with $1^\circ \times$
154 1° resolution. Apart from this, we also used daily mean merged precipitation data from the Global
155 Precipitation Mission (GPM) satellite in the present study. MERRA-2 data can be accessed through the
156 NASA Goddard Earth Sciences Data Information 135 Services Center (GES DISC;
157 <https://disc.gsfc.nasa.gov/>), while MODIS and GPM datasets were downloaded from the GIOVANNI
158 official website (<https://giovanni.gsfc.nasa.gov/giovanni/>).



159 **3 Results and Discussion**

160 **3.1 CMAQ model evaluation**

161 The statistical analysis of the CMAQ PM₁₀ modeling performance for the March 2010 SDS event is
162 shown in Table 2. DUST_Off and DUST_Default were similarly underestimated (Normalized Mean
163 Bias (NMB) = -65.02 % and -54.34 %, respectively), compared with the observed values, which is
164 consistent with the results of Dong et al. (2016) and Kong et al. (2021) that simulated moderate-
165 intensity dust events. The Dust_Refined_1 and Dust_Refined_2 simulations exhibited improved
166 accuracy (NMB = -41.43 % and -50.09 %, respectively), highlighting the importance of revising the
167 dust treatment before simulating the SDS event over a downwind region (Kong et al., 2021). Moreover,
168 the NMB for Refined_1 was lower than Refined_2 suggesting that simply calibrating the bulk soil
169 density is not as effective as calibrating for soil moisture fraction and dust emission speciation.
170 Eventually, Dust_Refined_3 resulted in the best performance (NMB = -30.73 %). Our results indicate
171 the importance of including both calibration methods in order to reduce the model uncertainty.

172 Figure 2 shows the in-situ and CMAQ-simulated PM₁₀ concentrations at Wanli station
173 (representing a background location in northern Taiwan) and Dongsha Island (representing the northern
174 South China Sea region) during 19-24 March 2010. In both locations, the Dust_Off trend vastly
175 underestimated the observations, whereas Dust_Default showed increased PM₁₀ concentrations but still
176 resulted in an underestimation. The PM₁₀ concentration at Wanli reached 1000 µg m³, which is the
177 maximum range of the instrument. CMAQ model predicted a peak PM₁₀ concentration of 868.8 µg m³,
178 thus was 13.1 % lower than the observation result, but should be considered a conservative estimate as
179 the observation amount may be underrepresented. At Dongsha Island, Dust_Refined_1 generated a
180 higher peak PM₁₀ value (371.6 µg m³) compared to Dust_Refined_2 (255.3 µg m³). Likewise,
181 Dust_Refined_3 generated a peak concentration of 524.4 µg m³, the highest among all of the simulation
182 scenarios, and only 5.9 % lower than the maximum observed PM₁₀ concentration of 557.0 µg m³.

183 Daily average modeled PM₁₀ concentration differences between Dust_Off and other simulations
184 over the East Asia region during 19-23 March 2010 is shown in Fig. 3. Dust_Default showed PM₁₀



185 concentration differences of approximately $200 \mu\text{g m}^{-3}$ over the source region of northwest China.
186 Dust_Refined_1 exhibited a difference of $\sim 600 \mu\text{g m}^{-3}$ over the source region, which was greater than
187 Dust_Refined_2. Overall, Dust_Refined_3 produced $> 800 \mu\text{g m}^{-3}$ difference, which was the highest
188 among the simulations. This result was further verified over the downwind region, where high PM_{10}
189 concentrations were observed in Taiwan and SCS regions (Fig. 3h). Further, we plotted MERRA-2
190 surface dust concentrations during 20-21 March 2010, which are shown in Fig. S1. The MERRA-2 data
191 indicated the dust plume only impacted Taiwan, while did not arrive at the SCS. Our model, on the
192 other hand, clearly (apparently) simulated the arrival of the dust plume to Dongsha Island, which is
193 consistent with 7-SEAS Dongsha Experiment-measured PM_{10} . Hence, this effort emphasizes the
194 importance of utilizing high-resolution simulations for depicting dust pollutant transport episodes.
195 Besides that, the wind speed and wind direction at different elevation levels play an important role in
196 dust transport. Uncertainty could be from this data if the wind component is poorly captured by the
197 satellite images used to generate the MERRA-2 reanalysis data.

198 In order to re-emphasize the precision of the dust treatment, we then implemented our
199 calibration method for other dust storm episodes that transported dust from northern Taiwan toward
200 southern Taiwan, which were documented by Wang et al. (2012). Hence, we carried out the 3-day
201 averaged sensitivity test over the East Asia region, estimated from d01 for four other notable dust storm
202 cases: 17-19 March 2005, 18-20 March 2006, 25-27 April 2009 and 20-22 March 2010 (Table 3).
203 Generally, DUST_Refined_3 performed well in simulating AOD over the East Asia region throughout
204 the four strong dust storm events. The average AOD value of the DUST_Refined_3 yielded an NMB of
205 -16.02% , which was markedly better than DUST_OFF (-26.09%), DUST_Default (-25.24%),
206 DUST_Refined_1 (-19.58%) and DUST_Refined_2 (-24.40%). Improvement of the modeled AOD by
207 approximately 10% was comparable with the result suggested by Dong et al. (2016). The temporal and
208 spatial distribution of CMAQ AOD showed the DUST_Refined_3 can modestly capture the dust storm
209 pattern as compared to MODIS-daily average AOD (Fig. S2). These results suggested DUST_refined_3
210 should be used for calibration as it successfully uplifts the dust aerosol at the source region and
211 simulates the notable dust cases over the East Asia region.



212 **3.2 Role of Central Mountain Range (CMR) on dust transport**

213 Figure 4 shows the spatial distribution of CMAQ estimated PM_{10} concentrations under Dust_Refined_3
214 simulations over East Asia during the March 2010 event. A low-pressure system of approximately 996
215 hPa over northwest China was associated with the uplifting of dust. As shown in Fig. 4b, a strong
216 pressure gradient led to strong wind speed generation, thus pushing the dust aerosol to move in the
217 southeast direction (Song et al., 2019; Kong et al., 2022). The dust arrived at massive concentrations in
218 transboundary regions such as southern China, Japan, Korea, and Taiwan, consistent with previous
219 studies (Lin et al., 2012; Bian et al., 2012) (Fig. 4c).

220 Figure 5 shows the CMAQ PM_{10} spatial distribution under Dust_Refined_3 simulations,
221 depicting the dust transport over Taiwan and Dongsha Island. On 16 UTC 20 March, one dust cloud
222 reached the surface in the Taiwan region (Fig. 5a) and split into two particular dust plumes due to the
223 Central Mountain Range (CMR) located in the center of Taiwan (Fig. 5b). At 04 UTC 21 March, the
224 first dust plume arrived at Dongsha Island, followed by the second 4 hours later (Fig. 5d, e). The model
225 result suggested the separated dust plumes originated from two different directions: the first one from
226 the Taiwan Strait (P1) and the second one from the Western Pacific Ocean (P2a) (Fig. 2). Meanwhile,
227 the measured PM_{10} concentration at Dongsha Island showed two peak values, at 15 UTC 21 March and
228 04 UTC 22 March 2010, respectively. The trends of the observed Dongsha peak value were consistent
229 with the CMAQ model results, where the model exhibited a clear PM_{10} peak at 06 UTC March 2010
230 (P2b in Fig. 2b). The “tail” of the dust plume swept over the South China Sea including Dongsha Island
231 due to the easterlies and northeasterly wind (Red arrow in Fig. 5e). Then, the dust cloud gradually
232 dissipated, leaving Dongsha Island and moving to southern China.

233 To better understand the role of the CMR on the SDS transport over SCS and Dongsha Island,
234 we carried out another simulation by removing the CMR and setting a zero altitude for the whole of
235 Taiwan Island within the WRF. We then examined the vertical profiles of the PM_{10} simulation, by
236 categorizing the model depiction into Cross A, Cross B, Cross C, and Cross D (Fig. 1b). The multiple
237 cross-section lines indicated the vertical dust pattern at different stages or locations, such as the dust
238 arrival at East China Sea (Cross A), Central Taiwan (Cross B), and the front (Cross C) and backward



239 (Cross D) of Dongsha Island across South China Sea. At 18 UTC on 20 March, preceding arrival to
240 Taiwan, both simulations with and without CMR showed the same pattern of PM₁₀ over the East China
241 Sea (ECS) (Fig. 6a, 6b). At 00 UTC on 21 March, the CMR of Taiwan effectively separated the dust
242 cloud into two parts as shown in the control run (Fig. 6c), which is not seen in the simulation without
243 CMR (Fig. 6d). Due to the role of the CMR, CMAQ simulations indicated two dust plumes arriving to
244 Dongsha Island (Cross C, Fig. 6e). Meanwhile, only one single plume was presented by the simulation
245 without CMR (Fig. 6f). At 15 UTC 21 March, both dust plumes were merged together and transported
246 to the west and northwest directions with respect to the easterly wind (Fig. 6g).

247 The role of CMR has been discussed in the literature, as it alters the strength of frontal
248 systems as they pass by Taiwan (Chien and Kuo, 2006). Also, due to the channel effect between the Wu
249 Yi Mountains in southeastern China and CMR in Taiwan, the air flow is forced to accelerate and causes
250 high intensity wind speeds through the Taiwan Strait (Lin et al., 2012a). Thus, the differential wind
251 speeds over the Taiwan Strait and eastern Taiwan, owing to the CMR, apparently caused uneven
252 “double plumes” over the Taiwan region.

253 **3.3 Role of the meteorological condition on dust transport**

254 The observed PM₁₀ over Dongsha Island (Fig. 2b) shows two separate peaks on March 20 and 22,
255 consistent with the reports of Wang et al. (2011). Our observed data showed minimal PM₁₀
256 concentrations between the two peaks, even though no precipitation was recorded over the site (Fig S3).
257 Figure 8 shows the daily precipitation over the downwind region. As discussed in Section 3.2, abundant
258 dust aerosol was transported through the Taiwan Strait and the Western Pacific Ocean, before arriving
259 at Dongsha Island. During 19-20 March 2010, no rainfall was captured by the satellite data over both
260 marine regions, resulting in the high PM₁₀ concentration of the first peak (Fig. 7a, b). On the other hand,
261 from 21 March to 22 March of 2010, heavy rainfall occurred in eastern Taiwan around the Western
262 Pacific Ocean. (Fig 7c, d). Based on the Global Precipitation Mission (GPM) satellite dataset,
263 precipitation in the region may have washed away dust aerosols before reaching the SCS and Dongsha
264 Island, resulting in lower PM₁₀ concentrations.



265 Regarding the importance of precipitation and wet deposition during the dust transport over the
266 downwind areas (Li et al., 2011; Kong et al., 2021), the spatial distribution of the modeled wet
267 deposition is shown in Fig. 8. Obviously, wet deposition was more intense over ECS than SCS, with
268 $\sim 20 \text{ mg m}^{-2}$ and $\sim 6 \text{ mg m}^{-2}$, respectively. However, in Fig. 2, the modeled PM_{10} concentration over
269 Wanli (northern Taiwan) was more underestimated than that at Dongsha Island (SCS). This situation
270 may be related to differences in the wet deposition magnitude over the different marine boundary layers.
271 Revising the CMAQ model deposition mechanism over the marine boundary layer was vital as
272 highlighted in our previous study (Kong et al., 2021). In the present work, we again suggest the
273 possibility of deposition flux variability over a different part of the marine boundary region (ECS vs.
274 SCS), which has not been mentioned by Kong et al. (2021).

275 **3.4 Role of a Typhoon on a dust storm event in April 2021**

276 Several studies have discussed the multiple dust storms over China in the spring of 2021 and the
277 associated dust emissions, transport/deposition, and radiative impact (Jin et al., 2022; Gui et al., 2022;
278 He et al., 2022; Liang et al., 2022; Tan et al., 2022). However, these studies only analyzed the incident
279 over the continental region. The SDS in transboundary areas, especially across the ocean marine
280 boundary layer, has not been closely tracked. As shown in Fig. 9(a), in the year 2021, three intensive
281 dust storms occurred during 14-18 March, 27-30 March and 15-17 April over China, which contained
282 the primary dust source region in each event (<https://www.aqistudy.cn/>). In the cities of northern China,
283 including Beijing, Hohhot and Taiyuan, the observed hourly PM_{10} concentrations vastly exceeded 1000
284 $\mu\text{g m}^{-3}$. Figure 9(b) shows the PM_{10} and $\text{PM}_{2.5}$ time series over Cape Fuguei (a background site in
285 northern Taiwan) during the spring of 2021 (<https://data.epa.gov.tw/>). Three PM_{10} peaks of of $165 \mu\text{g}$
286 m^{-3} , $116 \mu\text{g m}^{-3}$, and $246 \mu\text{g m}^{-3}$, were observed at 07 UTC 17 March, 13 UTC 22 March, and 22 UTC
287 18 April 2021, respectively. According to the Hybrid Single-Particle Lagrangian Integrated Trajectory
288 model (HYSPLIT) backward trajectory, the dust plumes arriving on 22 March and 18 April originated
289 from the Gobi Desert (Figure S4). The event on 17 March was from southern Japan, passed through the
290 marine boundary layer, and may have been due to local dust pollution from the local beach area. In
291 other words, out of three significant East Asian dust storms, one reached Taiwan and caused air quality



292 degradation over the region. The sudden increase in PM_{10} mass concentration that exceeded $200 \mu\text{g m}^{-3}$
293 indicated the high possibility of an SDS (Song et al., 2022).

294 Figure S5 shows the spatial distribution of AOD at 550 nm over East Asia from MERRA-2
295 reanalysis data and CMAQ Dust_Refined_3 simulations. Generally, the model reproduced well the dust
296 transport pattern shown by MERRA-2 reanalysis data during the dust event on 18 April. Figure 10
297 shows the spatial distribution of surface dust mass concentrations over East Asia during 18-19 April
298 2021. At 00 UTC on 18 April, the dust cloud arrived in Taiwan and approached the SCS. Meanwhile,
299 Typhoon Surigae, located east of the Philippines, accelerated and pulled a significant amount (up to 50
300 $\mu\text{g m}^{-3}$) of dust toward and into the typhoon center (Fig. 10b-e). Eventually, the dust mass
301 concentrations around the typhoon reduced (Fig. 10f-10h), while another fraction of the dust plume
302 passed through Taiwan and the Taiwan Strait, and was further transported towards the SCS.

303 The influence of the typhoon system on the dust aerosol can be further quantified by comparing
304 the MERRA-2 hourly averaged dust mass concentration over the ECS, Western Pacific Ocean (WPO),
305 and SCS (Fig. 11). The difference between the maximum values and the mean averaged (11-25 April
306 2021) dust mass concentrations was the highest over the WPO ($69.2 \mu\text{g m}^{-3}$), compared with ECS and
307 SCS ($13.6 \mu\text{g m}^{-3}$ and $14.2 \mu\text{g m}^{-3}$), indicating the remarkable dust removal by the typhoon. The
308 peripheral circulation on the southern side of the typhoon played a role in directing dust aerosol toward
309 the WPO and away from the ECS and SCS (Fig. 12a-d). This situation was due to the extreme wind
310 speed and the cyclonic rotation of the typhoon. The total precipitable water vapour shown by MERRA-
311 2 was intense around the eye of the typhoon, and the dust aerosol was shown to be washed out as it
312 passed through this area of the typhoon (Figure 12e-h). Moreover, the intensity of the total precipitation
313 was associated with the dust pattern (Li et al., 2011; Kong et al., 2021), as areas with more precipitation
314 (i.e. near the center) also contained lower dust concentrations (Fig. 10d-e).

315 As a result, the abnormal transport pattern can be attributed to the high-pressure system in
316 mainland China pushing the dust aerosol toward the downwind region (Chuang et al., 2008; Kong et al.,
317 2021), while the typhoon system over the Western Pacific Ocean accelerated transport of the dust plume



318 southward (Fig. 10i). CMAQ captured quite well the long-rang transport of dust toward the SCS and
319 Dongsha Island, where the plume passed through the Taiwan Strait (10j-10l). However, no dust aerosol
320 was found over the Western Pacific Ocean and the redirection of the dust plume by the typhoon, as
321 illustrated by the MERRA-2 data, was not reproduced by the model.

322 Figure 13a-d shows the CMAQ daily dust wet deposition over East Asia, where a cluster of wet
323 deposition was heavily distributed over the eastern Philippines. This large deposition flux could be
324 related to the heavy rainfall from the typhoon (Fig. 13i-l). Also, a similar pattern was found for the dry
325 deposition over the region, but with less intensity compared to the wet deposition (Fig. 13e-h).
326 Nevertheless, the dry deposition was spread widely over the western Pacific Ocean, consistent with the
327 daily mean wind speed over the region (Fig. 13m-p). Hence, the low dust concentration ($< 5 \mu\text{g m}^{-3}$)
328 over the WPO as predicted by CMAQ may have been driven by dry deposition associated with the
329 extreme wind speed triggered by the typhoon system.

330 Tropical cyclone (Typhoons/Hurricanes) normally occur over the WPO during the summer and
331 fall seasons, and tend to impact air quality and enhance the rainfall over the region (Lin et al., 2011;
332 Lam et al., 2018; Lin et al., 2021). Typhoons have been shown to increase aerosols over central Taiwan
333 and create strong easterly flow causing stable weather conditions and weak wind speed, on the lee side
334 of the CMR, i.e. in western Taiwan (Lin et al. 2021). The present study highlights the ability of a
335 typhoon to remove dust aerosol that have been transported thousands of kilometers from northwest
336 China. This enhanced wet deposition flux is consistent with Kong et al. (2021) that showed the
337 influence of a rainfall belt to increase dust deposition over ECS.

338 The daily mean surface dust mass concentrations on 18 March 2005 (D1), 19 March 2006 (D2),
339 24 April 2009 (D3), 21 March 2010 (D4) and 18 April 2021 (D5) are displayed in Fig. 14. Episode D4
340 was a more intense dust plume compared to D1, D2, D3 and D5 as D4 was the SDS while the other
341 episodes were just the regular dust storm (Wang et al., 2012; Wang et al., 2021). Episodes D1, D2, D3
342 and D4 revealed a common/typical dust transport pattern with the initial dust arrival at ECS, and then
343 Taiwan Strait and WPO. However, in episode D5, the dust plume was only distributed over the ECS



344 and Taiwan Strait, and near-zero dust concentration was observed over the WPO. Hence, we revealed
345 an influence of a typhoon on dust transport patterns over East Asia, and highlighted the associated
346 excessive rainfall as an extraordinary, albeit irregular, removal mechanism over the WPO. As a result of
347 this variable transport pattern, the accuracy of the dust model in simulating the dust event encountered a
348 large degree of uncertainty, which is compounded by uncertainties in the dust emission scheme and dust
349 removal process (Kong et al., 2021; He et al., 2022). For instance, dust emission at the source region
350 can vary due to the different calibration methods, revealing the use of the dust scheme is not
351 straightforward and extensive testing should be carried out in order to achieve a better model
352 performance. Moreover, over the downwind region, the specific meteorological situation including the
353 wind speed, rainfall distribution, and extreme weather pattern could impact the transport pattern, and
354 further influence the dust model precision.

355 **4. Summary and Conclusions**

356 Dust storm outbreaks in East Asia are an irregular occurrence, but can rapidly deteriorate air quality
357 over a wide swath of the continent, causing severe health and environmental problems. Long-range
358 transport of East Asian dust to the South China Sea and the source emission, transport pattern and
359 deposition that facilitate these episodes have been largely overlooked. In this study, we combined
360 ground observations from the 7-SEAS Dongsha Experiment, MERRA-2 reanalysis, and MODIS
361 satellite images for evaluation and improvement of the CMAQ dust model for cases of EAD reaching
362 the Taiwan region, including Dongsha Island in the northern South China Sea.

363 We improved the dust treatment in the CMAQ model by implementing a refined aerosol profile,
364 the soil moisture fraction (Kong et al., 2021), and the bulk density of different soil types (Liu et al.,
365 2021). Based on the latest refined dust model, we simulated the long-range transport of a Super Dust
366 Storm (SDS) during 18-24 March 2010, and several significant dust storm events on 17-19 March 2005,
367 18-20 March 2006, 25-27 April 2009 and 15-21 April 2021, and detailed their respective transport
368 mechanisms. For the 2010 March SDS, our model suggested the dust simulation over Taiwan and
369 Dongsha Island was optimized with the dust scheme considering all the calibration methods, which is



370 the Dust_Refined_3 that provided the best NMB (-30.73 %), compared to the calibration recommended
371 by Kong et al. (2021) (-41.43 %) and Liu et al. (2021) (-50.09 %). The SDS transport mechanism over
372 Dongsha Island in the South China Sea was influenced by the CMR in Taiwan. A “double plume” effect
373 was proposed, i.e. the dust plume split with a portion passing through the Taiwan Strait (west side of
374 CMR) and the other through the Western Pacific Ocean region (east side of CMR). Also,
375 Dust_Refined_3 treatment provided an optimized AOD simulation value during the significant dust
376 cases on March 2005, March 2006, April 2009 and March 2010.

377 In spring 2021, multiple East Asian dust storms occurred over the region after a period of
378 relative infrequency of nearly 12 years. One episode reached northern Taiwan, and deteriorated the
379 ambient air quality, resulting in a maximum PM₁₀ concentration of 246 μg m⁻³. In contrast with previous
380 dust episodes that have reached the Taiwan region, both the satellite dataset and model result illustrated
381 a “double synoptic pattern” driven by a high-pressure system over the continent and a typhoon system
382 in the Western Pacific Ocean. The dust plume was pushed by the high-pressure system toward Taiwan,
383 and at the same time by typhoon “Surigae”, resulting in the dust cloud splitting and a portion drawn in
384 by the typhoon circulation towards its center. This unique mechanism appeared to be accompanied by
385 increased dry or wet deposition of the dust particles over the WPO.

386 **Data Availability**

387 MERRA-2 data are available online through the NASA Goddard Earth Sciences Data Information
388 Services Center (GES DISC; <https://disc.gsfc.nasa.gov>; last access: 08 June 2023). MODIS data used in
389 this study are available at <https://asdc.larc.nasa.gov/>(last access: 08 June 2023). The GPM dataset were
390 downloaded from the GIOVANNI official website at <https://giovanni.gsfc.nasa.gov/giovanni/> (last
391 access: 08 June 2023). The observational data at Dongsha can be ordered by contacting corresponding
392 authors.



393 **Author Contribution**

394 **Steven Soon-Kai Kong:** Conceptualization; Data curation; Formal analysis; Investigation;
395 Methodology; Software; Validation; Visualization; Writing – original draft; Writing – review and
396 editing.

397 **Saginela Ravindra Babu:** Conceptualization; Investigation; Methodology; Formal analysis; Writing –
398 review and editing.

399 **Sheng-Hsiang Wang:** Formal analysis; Data curation.

400 **Stephen M. Griffith:** Writing – review and editing.

401 **Jackson Hian-Wui Chang:** Data curation and software.

402 **Ming-Tung Chuang:** Data curation.

403 **Guey-Rong Sheu:** Funding acquisition; Resources.

404 **Neng-Huei Lin:** Conceptualization; Visualization; Supervision; Funding acquisition; Resources;
405 Writing – review and editing.

406 **Competing Interest**

407 The authors declare that they have no conflict of interest.

408 **Acknowledgments**

409 We acknowledged the Ministry of Science and Technology of Taiwan, under Project No. MSTC111-
410 2811-M-008-069 for supporting the research. We also acknowledged the staff at Dongsha Island, and
411 EPA Taiwan for the provision of the ground-based measurement datasets. We are also thankful to
412 MERRA-2 and MODIS for the satellite product.

413 **References**

414 Appel, K.W., Pouliot, G.A., Simon, H., Sarwar, G., Pye, H.O.T., Napelenok, S.L., Akhtar, F. and
415 Roselle, S.J.: Evaluation of dust and trace metal estimates from the Community Multiscale Air Quality



- 416 (CMAQ) model version 5.0. *Geoscientific Model Development*, 6, 4, 883–899,
417 <https://doi.org/10.5194/gmd-6-883-2013>, 2013.
- 418 Bian, H., Tie, X., Cao, J., Ying, Z., Han, S., and Xue, Y.: Analysis of a severe dust storm event over
419 China: Application of the WRF-dust model, *Aerosol and Air Quality Research*, 11, 419–428,
420 <https://doi.org/10.4209/aaqr.2011.04.0053>, 2011.
- 421 Chen, C., Mao, Z., Tang, F., Han, G., and Jiang, Y.: Declining riverine sediment input impact on spring
422 phytoplankton bloom off the Yangtze River Estuary from 17-year satellite observation, *Continental
423 Shelf Research*, 135, 86–91, <https://doi.org/10.1016/j.csr.2017.01.012>, 2017a.
- 424 Chen, S., Huang, J., Kang, L., Wang, H., Ma, X., He, Y., Yuan, T., Yang, B., Huang, Z., and Zhang, G.:
425 Emission, transport, and radiative effects of mineral dust from the Taklimakan and Gobi deserts:
426 Comparison of measurements and model results, *Atmospheric Chemistry and Physics*, 17, 2401–2421,
427 <https://doi.org/10.5194/acp-17-2401-2017>, 2017b.
- 428 Chien, F.-C. and Kuo, Y.-H.: Topographic Effects on a Wintertime Cold Front in Taiwan, *Monthly
429 Weather Review*, 134, 3297–3316, <https://doi.org/10.1175/mwr3255.1>, 2006.
- 430 Chow, K. C., Su, L., Fung, J. C. H., Ma, H., and Lau, A. K. H.: Numerical modeling of a strong dust
431 event over the south China region in March 2010, *Meteorology and Atmospheric Physics*, 126, 119–138,
432 <https://doi.org/10.1007/s00703-014-0338-0>, 2014.
- 433 Dong, X., Fu, J. S., Huang, K., Tong, D., and Zhuang, G.: Model development of dust emission and
434 heterogeneous chemistry within the Community Multiscale Air Quality modeling system and its
435 application over East Asia, *Atmospheric Chemistry and Physics*, 8157–8180,
436 <https://doi.org/10.5194/acp-16-8157-2016>, 2016.
- 437 Dong, X., Fu, J. S., Huang, K., Zhu, Q., and Tipton, M.: Regional Climate Effects of Biomass Burning
438 and Dust in East Asia: Evidence From Modeling and Observation, *Geophysical Research Letters*, 46,
439 11490–11499, <https://doi.org/10.1029/2019GL083894>, 2019.
- 440 Duce, R. A., Liss, P. S., Merrill, J. T., Atlas, E. L., Buat-Menard, P., Hicks, B. B., Miller, J. M.,
441 Prospero, J. M., Arimoto, R., Church, T. M., Ellis, W., Galloway, J. N., Hansen, L., Jickells, T. D.,
442 Knap, A. H., Reinhardt, K. H., Schneider, B., Soudine, A., Tokos, J. J., Tsunogai, S., Wollast, R., and



- 443 Zhou, M.: The atmospheric input of trace species to the world ocean, *Global Biogeochemical Cycles*, 5,
444 193–259, <https://doi.org/10.1029/91GB01778>, 1991.
- 445 Foroutan, H., Young, J., Napelenok, S., Ran, L., Appel, K., Gilliam, R., and Pleim, J.: Journal of
446 Advances in Modeling Earth Systems, *Journal of Advances in Modeling Earth Systems*, 9, 585–606,
447 <https://doi.org/10.1002/2013MS000282>.Received, 2017.
- 448 Gelaro, R., McCarty, W., Suárez, M. J., Todling, R., Molod, A., Takacs, L., Randles, C. A., Darmenov,
449 A., Bosilovich, M. G., Reichle, R., Wargan, K., Coy, L., Cullather, R., Draper, C., Akella, S., Buchard,
450 V., Conaty, A., da Silva, A. M., Gu, W., Kim, G. K., Koster, R., Lucchesi, R., Merkova, D., Nielsen, J.
451 E., Partyka, G., Pawson, S., Putman, W., Rienecker, M., Schubert, S. D., Sienkiewicz, M., and Zhao, B.:
452 The modern-era retrospective analysis for research and applications, version 2 (MERRA-2), *Journal of*
453 *Climate*, 30, 5419–5454, <https://doi.org/10.1175/JCLI-D-16-0758.1>, 2017.
- 454 Griffin, D. and Kellogg, C.: Dust Storms and Their Impact on Ocean and Human Health: Dust in
455 Earth's Atmosphere, *EcoHealth*, 1, <https://doi.org/10.1007/s10393-004-0120-8>, 2004.
- 456 Gui, K., Yao, W., Che, H., An, L., Zheng, Y., Li, L., Zhao, H., Zhang, L., Zhong, J., Wang, Y., and
457 Zhang, X.: Record-breaking dust loading during two mega dust storm events over northern China in
458 March 2021: aerosol optical and radiative properties and meteorological drivers, *Atmospheric*
459 *Chemistry and Physics*, 22, 7905–7932, <https://doi.org/10.5194/acp-22-7905-2022>, 2022.
- 460 Guo, J., Lou, M., Miao, Y., Wang, Y., Zeng, Z., Liu, H., He, J., Xu, H., Wang, F., Min, M., and Zhai, P.:
461 Trans-Pacific transport of dust aerosols from East Asia: Insights gained from multiple observations
462 and modeling, *Environmental Pollution*, 230, 1030–1039, <https://doi.org/10.1016/j.envpol.2017.07.062>,
463 2017.
- 464 Han, X., Ge, C., Tao, J., Zhang, M., and Zhang, R.: Air quality modeling for a strong dust event in East
465 Asia in March 2010, *Aerosol and Air Quality Research*, 12, 615–628,
466 <https://doi.org/10.4209/aaqr.2011.11.0191>, 2012.
- 467 He, Y., Yi, F., Yin, Z., Liu, F., Yi, Y., and Zhou, J.: Mega Asian dust event over China on 27–31 March
468 2021 observed with space-borne instruments and ground-based polarization lidar, *Atmospheric*
469 *Environment*, 285, 119238, <https://doi.org/10.1016/j.atmosenv.2022.119238>, 2022.



- 470 Huang, J., Wang, T., Wang, W., Li, Z., and Yan, H.: Journal of Geophysical Research : Atmospheres,
471 398–416, <https://doi.org/10.1002/2014JD021796>.Received, 2014.
- 472 Jiang, N., Dong, Z., Xu, Y., Yu, F., Yin, S., Zhang, R., and Tang, X.: Characterization of PM10and
473 PM2.5source profiles of fugitive dust in Zhengzhou, China, Aerosol and Air Quality Research, 18, 314–
474 329, <https://doi.org/10.4209/aaqr.2017.04.0132>, 2018.
- 475 Jin, J., Pang, M., Segers, A., Han, W., Fang, L., Li, B., Feng, H., Lin, H. X., and Liao, H.: Inverse
476 modeling of the 2021 spring super dust storms in East Asia, Atmospheric Chemistry and Physics, 22,
477 6393–6410, <https://doi.org/10.5194/acp-22-6393-2022>, 2022.
- 478 Jing, Y., Zhang, P., Chen, L., and Xu, N.: Integrated analysis of dust transport and budget in a severe
479 asian dust event, Aerosol and Air Quality Research, 17, 2390–2400,
480 <https://doi.org/10.4209/aaqr.2017.05.0170>, 2017.
- 481 Kong, S. S.-K., Pani, S. K., Griffith, S. M., Ou-Yang, C.-F., Babu, S. R., Chuang, M.-T., Ooi, M. C. G.,
482 Huang, W.-S., Sheu, G.-R., and Lin, N.-H.: Distinct transport mechanisms of East Asian dust and the
483 impact on downwind marine and atmospheric environments, Science of The Total Environment, 827,
484 154255, <https://doi.org/10.1016/j.scitotenv.2022.154255>, 2022.
- 485 Kong, S. S., Fu, J. S., Dong, X., Chuang, M., Chel, M., Ooi, G., Huang, W., Griffith, S. M., Kumar, S.,
486 and Lin, N.: Sensitivity analysis of the dust emission treatment in CMAQv5 . 2 . 1 and its application to
487 long-range transport over East Asia, Atmospheric Environment, 118441,
488 <https://doi.org/10.1016/j.atmosenv.2021.118441>, 2021.
- 489 Lam, Y. F., Cheung, H. M., and Ying, C. C.: Impact of tropical cyclone track change on regional air
490 quality, Science of the Total Environment, 610–611, 1347–1355,
491 <https://doi.org/10.1016/j.scitotenv.2017.08.100>, 2018.
- 492 Li, J., Han, Z., Zhang, R., and Asia, E.: Model study of atmospheric particulates during dust storm
493 period in March 2010 over East Asia, Atmospheric Environment, 45, 3954–3964,
494 <https://doi.org/10.1016/j.atmosenv.2011.04.068>, 2011.
- 495 Liang, L., Han, Z., Li, J., Xia, X., Sun, Y., Liao, H., Liu, R., and Liang, M.: Emission , transport ,
496 deposition , chemical and radiative impacts of mineral dust during severe dust storm periods in March



497 2021 over East Asia, *Science of the Total Environment*, 852, 158459,
498 <https://doi.org/10.1016/j.scitotenv.2022.158459>, 2022.

499 Lin, C., Sheng, Y., Chen, W., Wang, Z., Kuo, C., Chen, W., and Yang, T.: The impact of channel effect
500 on Asian dust transport dynamics: a case in southeastern Asia, *Atmospheric Chemistry and Physics*,
501 271–285, <https://doi.org/10.5194/acp-12-271-2012>, 2012a.

502 Lin, C., Chou, C. C. K., Wang, Z., Lung, S., Lee, C., Yuan, C., Chen, W., Chang, S., Hsu, S., Chen, W.,
503 and Chen, S.: Impact of different transport mechanisms of Asian dust and anthropogenic pollutants to
504 Taiwan, *Atmospheric Environment*, 60, 403–418, <https://doi.org/10.1016/j.atmosenv.2012.06.049>,
505 2012b.

506 Lin, C. Y., Hsu, H. M., Shengl, Y. F., Kuo, C. H., and Liou, Y. A.: Mesoscale processes for super heavy
507 rainfall of typhoon Morakot (2009) over southern Taiwan, *Atmospheric Chemistry and Physics*, 11,
508 345–361, <https://doi.org/10.5194/acp-11-345-2011>, 2011.

509 Lin, C. Y., Sheng, Y. F., Chen, W. C., Chou, C. C. K., Chien, Y. Y., and Chen, W. M.: Air quality
510 deterioration episode associated with a typhoon over the complex topographic environment in central
511 Taiwan, *Atmospheric Chemistry and Physics*, 21, 16893–16910, [https://doi.org/10.5194/acp-21-16893-](https://doi.org/10.5194/acp-21-16893-2021)
512 2021, 2021.

513 Lin, N.-H., Tsay, S.-C., Maring, H. B., Yen, M.-C., Sheu, G.-R., Wang, S.-H., Chi, K. H., Chuang, M.-
514 T., Ou-Yang, C.-F., Fu, J. S., Reid, J. S., Lee, C.-T., Wang, L.-C., Wang, J.-L., Hsu, C. N., Sayer, A.
515 M., Holben, B. N., Chu, Y.-C., Nguyen, X. A., Sopajaree, K., Chen, S.-J., Cheng, M.-T., Tsuang, B.-J.,
516 Tsai, C.-J., Peng, C.-M., Schnell, R. C., Conway, T., Chang, C.-T., Lin, K.-S., Tsai, Y. I., Lee, W.-J.,
517 Chang, S.-C., Liu, J.-J., Chiang, W.-L., Huang, S.-J., Lin, T.-H., and Liu, G.-R.: An overview of
518 regional experiments on biomass burning aerosols and related pollutants in Southeast Asia: From
519 BASE-ASIA and the Dongsha Experiment to 7-SEAS, *Atmos. Environ.*, 78, 1–19,
520 <https://doi.org/10.1016/j.atmosenv.2013.04.066>, 2013

521 Liu, S., Xing, J., Sahu, S. K., Liu, X., Liu, S., Jiang, Y., Zhang, H., Li, S., Ding, D., Chang, X., and
522 Wang, S.: Wind-blown dust and its impacts on particulate matter pollution in Northern China: Current
523 and future scenarios, *Environmental Research Letters*, 16, 114041, [https://doi.org/10.1088/1748-](https://doi.org/10.1088/1748-9326/ac31ec)
524 9326/ac31ec, 2021.



- 525 Park, S., Choe, A., and Park, M.: A simulation of Asian dust events in March 2010 by using the
526 ADAM2 model, *Theoretical and Applied Climatology*, 107, 491–503, [https://doi.org/10.1007/s00704-](https://doi.org/10.1007/s00704-011-0494-9)
527 011-0494-9, 2012.
- 528 Shao, Y. and Dong, C. H.: A review on East Asian dust storm climate, modelling and monitoring,
529 *Global and Planetary Change*, 52, 1–22, <https://doi.org/10.1016/j.gloplacha.2006.02.011>, 2006.
- 530 Song, L., Bi, X., Zhang, Z., Li, L., Dai, Q., Zhang, W., Li, H., Wang, X., Liang, D., Feng, Y.: Impact of
531 sand and dust storms on the atmospheric environment and its source in Tianjin, China, *Sci Total Environ*,
532 825, <https://doi.org/10.1016/j.scitotenv.2022.153980>, 2022.
- 533 Song, P., Fei, J., Li, C., and Huang, X.: Simulation of an Asian Dust Storm Event in May 2017,
534 *Atmosphere*, 10(3), 135, <https://doi.org/10.3390/atmos10030135>, 2019.
- 535 Sullivan, H.: Beijing hit by third sandstorm in five weeks. [https://www.the-guardian.com/world/](https://www.the-guardian.com/world/2021/apr/16/beijing-hit-by-third-sandstorm-in-just-over-a-month)
536 2021/ apr/ 16/ beijing- hit- by- third- sandstorm- in- just- over-a- month, last access: 25 June 2021
- 537 Tan, S., Li, J., Che, H., Chen, B., and Wang, H.: Transport of East Asian dust storms to the marginal
538 seas of China and the southern North Pacific in spring 2010, *Atmospheric Environment*, 148, 316–328,
539 <https://doi.org/10.1016/j.atmosenv.2016.10.054>, 2017.
- 540 Tang, W., Dai, T., Cheng, Y., Wang, S., and Liu, Y.: A Study of a Severe Spring Dust Event in 2021
541 over East Asia with WRF-Chem and Multiple Platforms of Observations, *Remote Sensing*, 14, 3795,
542 <https://doi.org/10.3390/rs14153795>, 2022.
- 543 Uno, I., Osada, K., Yumimoto, K., Wang, Z., Itahashi, S., Pan, X., Hara, Y., Yamamoto, S., and
544 Nishizawa, T.: Importance of long-range nitrate transport based on long-term observation and modeling
545 of dust and pollutants over East Asia, *Aerosol and Air Quality Research*, 17, 3052–3064,
546 <https://doi.org/10.4209/aaqr.2016.11.0494>, 2017.
- 547 Vukovich, J. M. and Pierce, T.: The Implementation of BEIS3 within the SMOKE modeling framework,
548 1–7, 1988.
- 549 Wang, J., Gui, H., An, L., Hua, C., Zhang, T., and Zhang, B.: Modeling for the source apportionments
550 of PM10 during sand and dust storms over East Asia in 2020, *Atmospheric Environment*, 267, 118768,
551 <https://doi.org/10.1016/j.atmosenv.2021.118768>, 2021.



552 Wang, S., Tsay, S., Lin, N., Hsu, N. C., Bell, S. W., Li, C., Ji, Q., Jeong, M., Hansell, R. A., Welton, E.
553 J., Holben, B. N., Sheu, G., Chu, Y., Chang, S., Liu, J., and Chiang, W.: First detailed observations of
554 long-range transported dust over the northern South China Sea, *Atmospheric Environment*, 45, 4804–
555 4808, <https://doi.org/10.1016/j.atmosenv.2011.04.077>, 2011.

556 Wang, S. H., Hsu, N. C., Tsay, S. C., Lin, N. H., Sayer, A. M., Huang, S. J., and Lau, W. K. M.: Can
557 Asian dust trigger phytoplankton blooms in the oligotrophic northern South China Sea?, *Geophysical*
558 *Research Letters*, 39, <https://doi.org/10.1029/2011GL050415>, 2012.

559 Yao, W., Gui, K., Wang, Y., Che, H., and Zhang, X.: Identifying the dominant local factors of 2000–
560 2019 changes in dust loading over East Asia, *Sci. Total Environ.*, 777, 146064,
561 <https://doi.org/10.1016/j.scitotenv.2021.146064>, 2021.

562 Zhao, J., Zhang, F., Xu, Y., Chen, J., Yin, L., Shang, X., and Xu, L.: Chemical Characteristics of
563 Particulate Matter during a Heavy Dust Episode in a Coastal City , Xiamen , 2010, *Aerosol and Air*
564 *Quality Research*, 299–308, <https://doi.org/10.4209/aaqr.2010.09.0073>, 2011.

565

566

567

568

569

570

571

572

573

574

575

576

577

578

579

580

581

582

583

584

585



586 **Table 1** Summary of the design of the simulations used in the present study.

Scenarios	Descriptions
Dust_Off	Without in-line calculation of dust.
Dust_Default	With the new default wind-blown dust treatment (Foroutan et al., 2017).
Dust_Refined_1	Refined the soil moisture factor and the dust emission speciation profile for the Gobi Desert as suggested by Kong et al. (2021).
Dust_Refined_2	Refined the bulb soil density according to China's soil type as suggested by Liu et al. (2021).
Dust_Refined_3	Considering the both of Dust_Refined_1 and Dust_Refined_2.

587

588

589 **Table 2** Statistical index for PM₁₀ concentration during 19-23 March 2010, for Taiwan Island (Banqiao,
590 Pinzhen, Hsinchu, Xitun, Xinying, Zhuoyin, Daliao) and Dongsha Island.

	Benchmark	Off	Default	Refined_1	Refined_2	Refined_3
MeanObs		176.47	176.47	176.47	176.47	176.47
MeanMod		50.99	64.71	82.12	70.60	96.23
NMSE		2.11	1.52	1.17	1.36	1.03
MFB	± 60%	-65.67	-55.77	-45.39	-52.34	-38.82
NMB	± 85%	-65.02	-54.34	-41.34	-50.09	-30.73
NME	85%	65.02	60.35	57.44	59.16	55.24
FAC2	0.5–2.0	0.70	0.83	0.98	0.87	1.11
R	> 0.35	0.25	0.37	0.39	0.41	0.38

591 Note: the definition of the statistical formulas NMSE: Normalized Mean Square Error; MNB: Mean
592 Normalized Bias; NMB: Normalized Mean Bias; NME: Normalized Mean Error; FAC2: Factor of Two;
593 R: Correlation Coefficient.

594

595

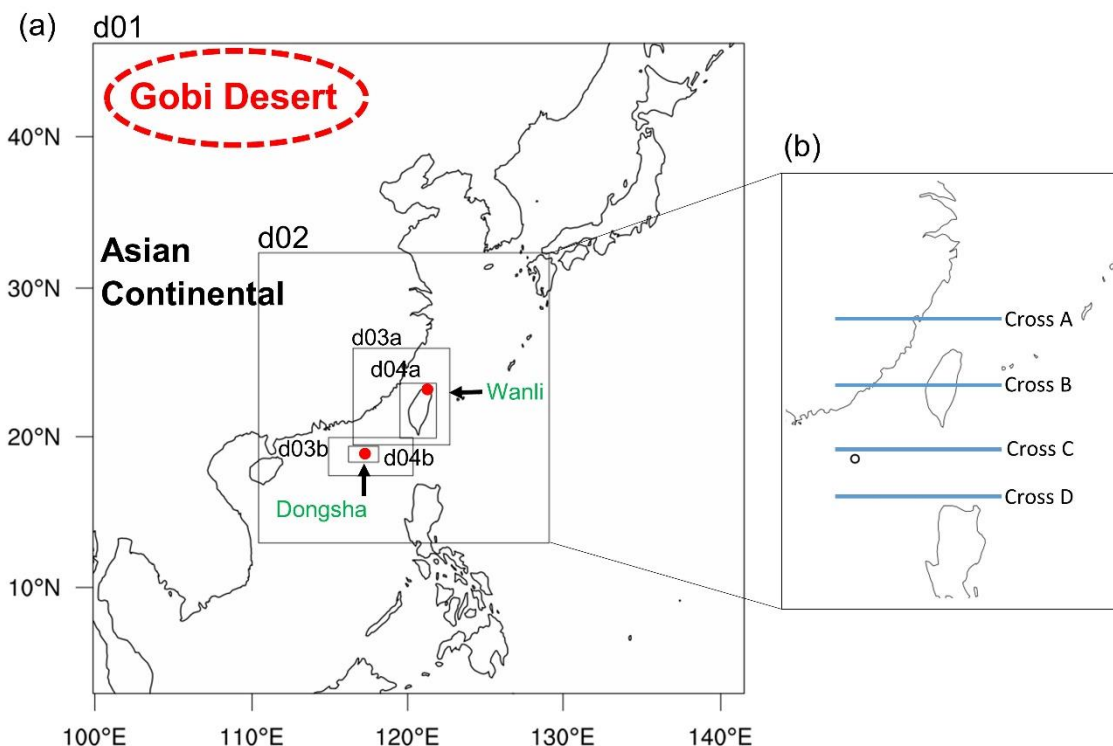
596 **Table 3** CMAQ AOD evaluation against MODIS daily observation with Normalized Mean Bias (NMB)
597 for the multiple simulation scenarios during the dust storm episode of Mar2005 (16-20 March 2005),
598 Mar2006 (17-21 March 2006), Apr2009 (24-28 April 2009) and Mar2010 (19-23 March 2010).

Cases	Mar2005	Mar2006	Apr2009	Mar2010	Mean
Dust_Off	-13.04	-30.84	-37.30	-49.26	-26.09
Dust_Default	-13.04	-30.84	-37.30	-45.03	-25.24
Dust_Refined_1	-9.70	-27.95	-27.90	-32.35	-19.58
Dust_Refined_2	-13.04	-30.84	-37.30	-40.80	-24.40
Dust_Refined_3	-6.35	-25.07	-24.76	-23.89	-16.02

599

600

601



602

603

604

605

606

607

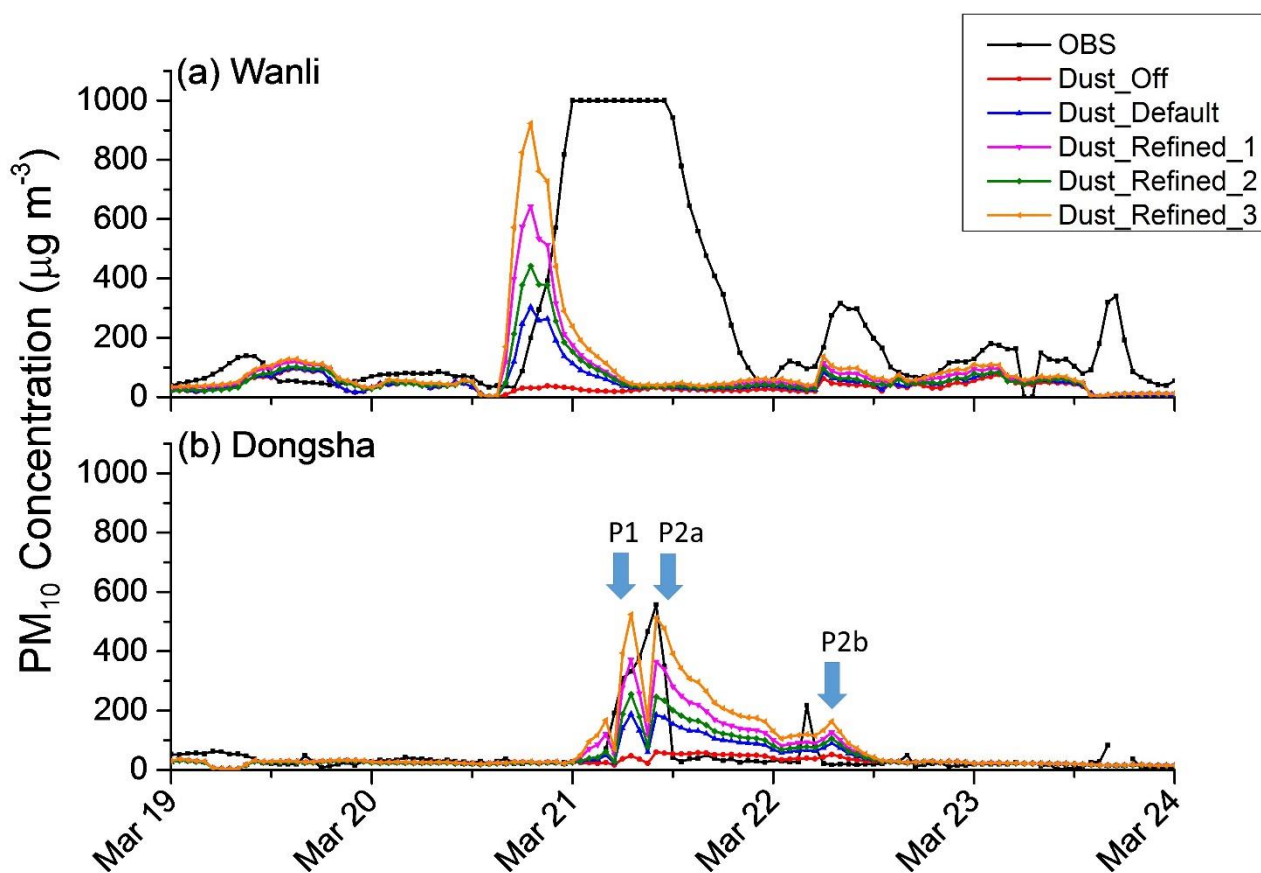
608

609

610

611

Figure 1: (a) Modeling domain configuration used in the present study. The red dot representing the location of the observation sites at Wanli and Dongsha. (b) The blue lines represent the transects that the dust plumes travelled along in this studies that are discussed in **Section 3**.



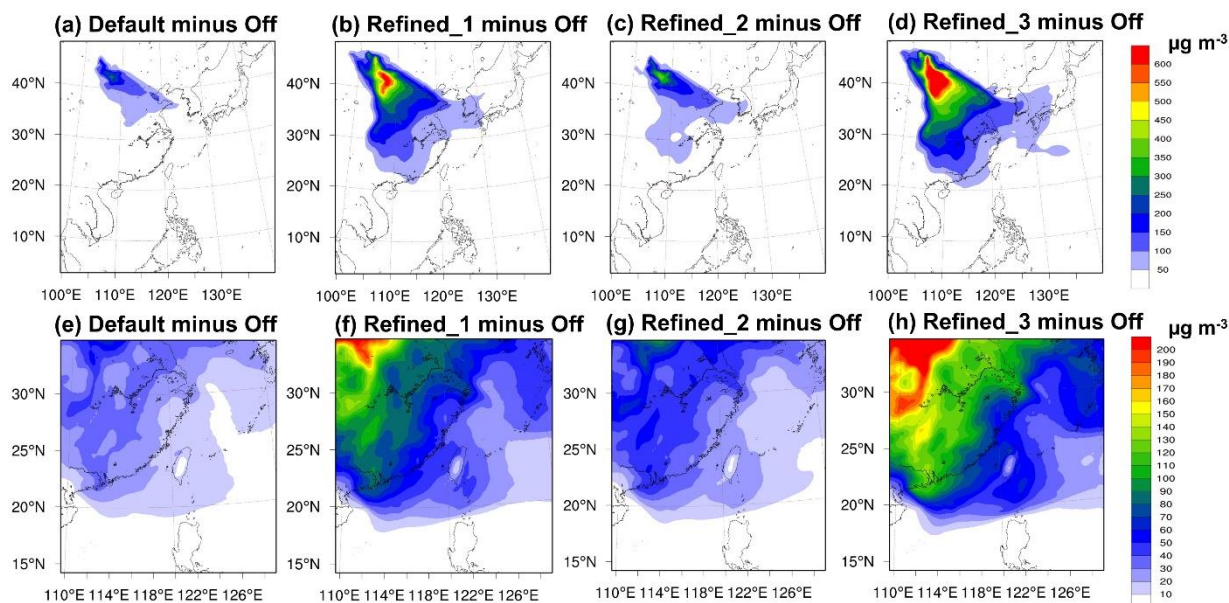
612
613

614 **Figure 2:** Time series of observed PM₁₀ concentrations over Wanli sites and Dongsha Island during 19-
615 23 March 2010.

616
617
618
619
620
621
622
623
624
625
626
627
628
629
630
631
632

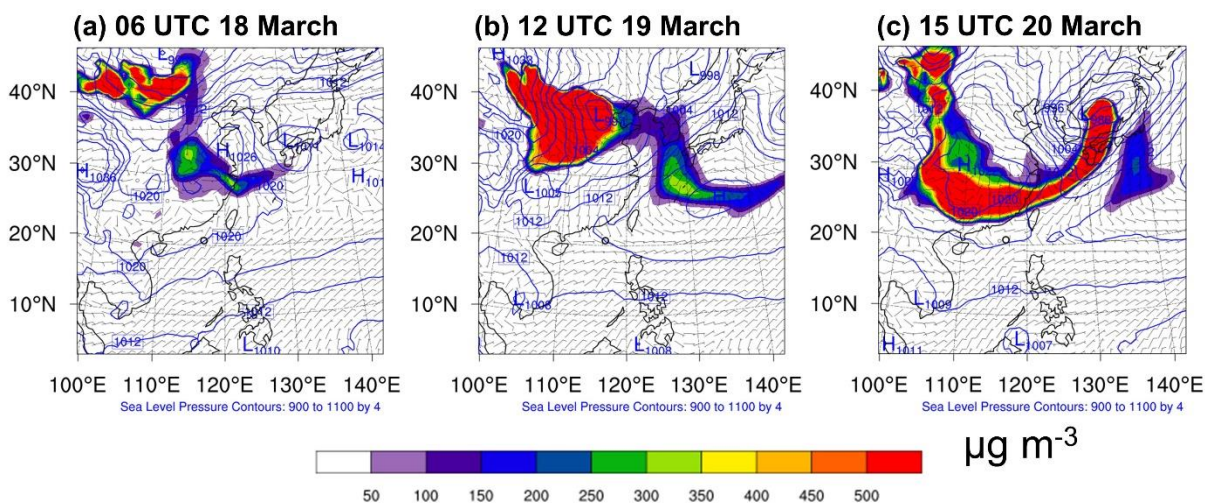


633
634



635
636
637
638
639
640
641
642
643

Figure 3: The difference of the daily average modeled PM₁₀ concentrations over d01 (a–d) and d02 (e–h) between Dust_Off, and Dust_Default, Dust_Refined_1, Dust_Refined_2 and Dust_Refined_3, respectively.

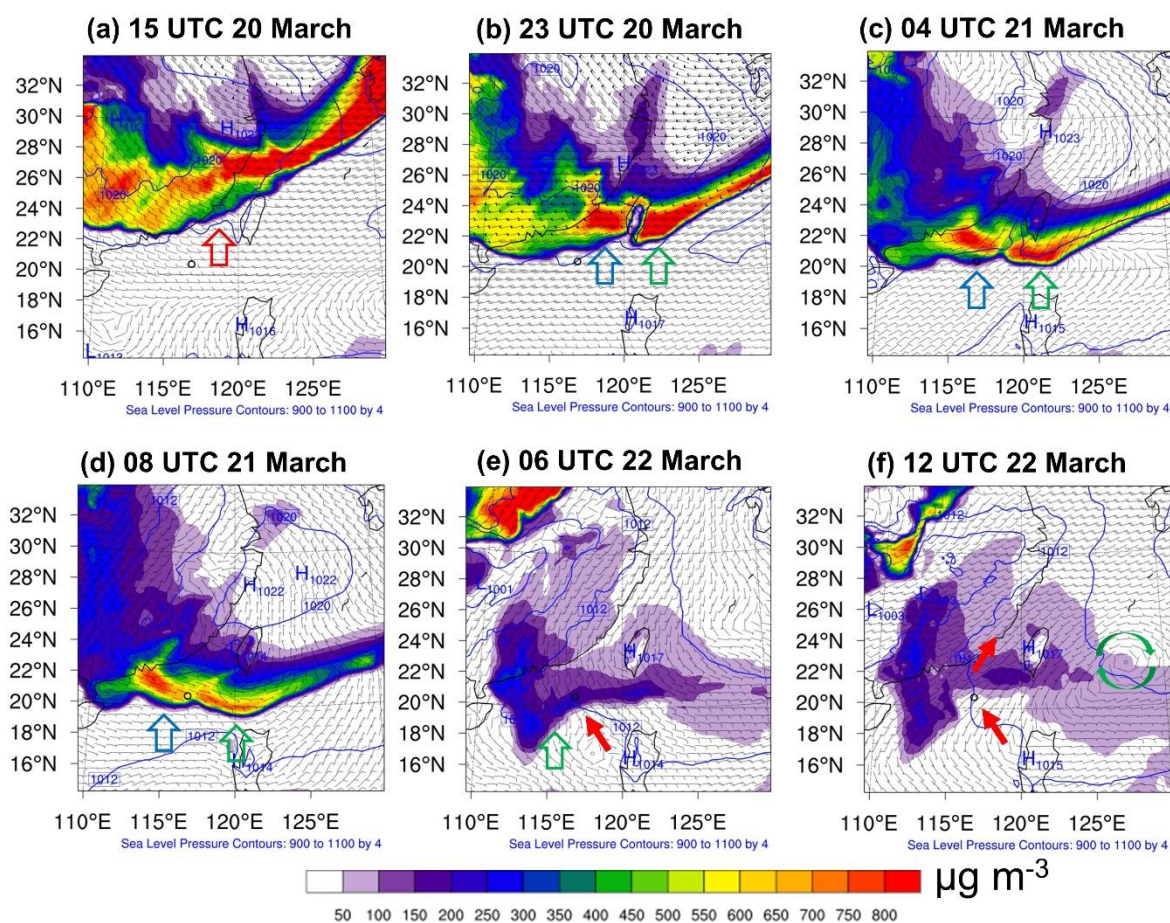


644
645
646
647

Figure 4: Spatial distribution of the simulated dust aerosol during (a) 06 UTC 18 March, (b) 12 UTC 19 March and (c) 15 UTC 20 March, in the year of 2010.



648



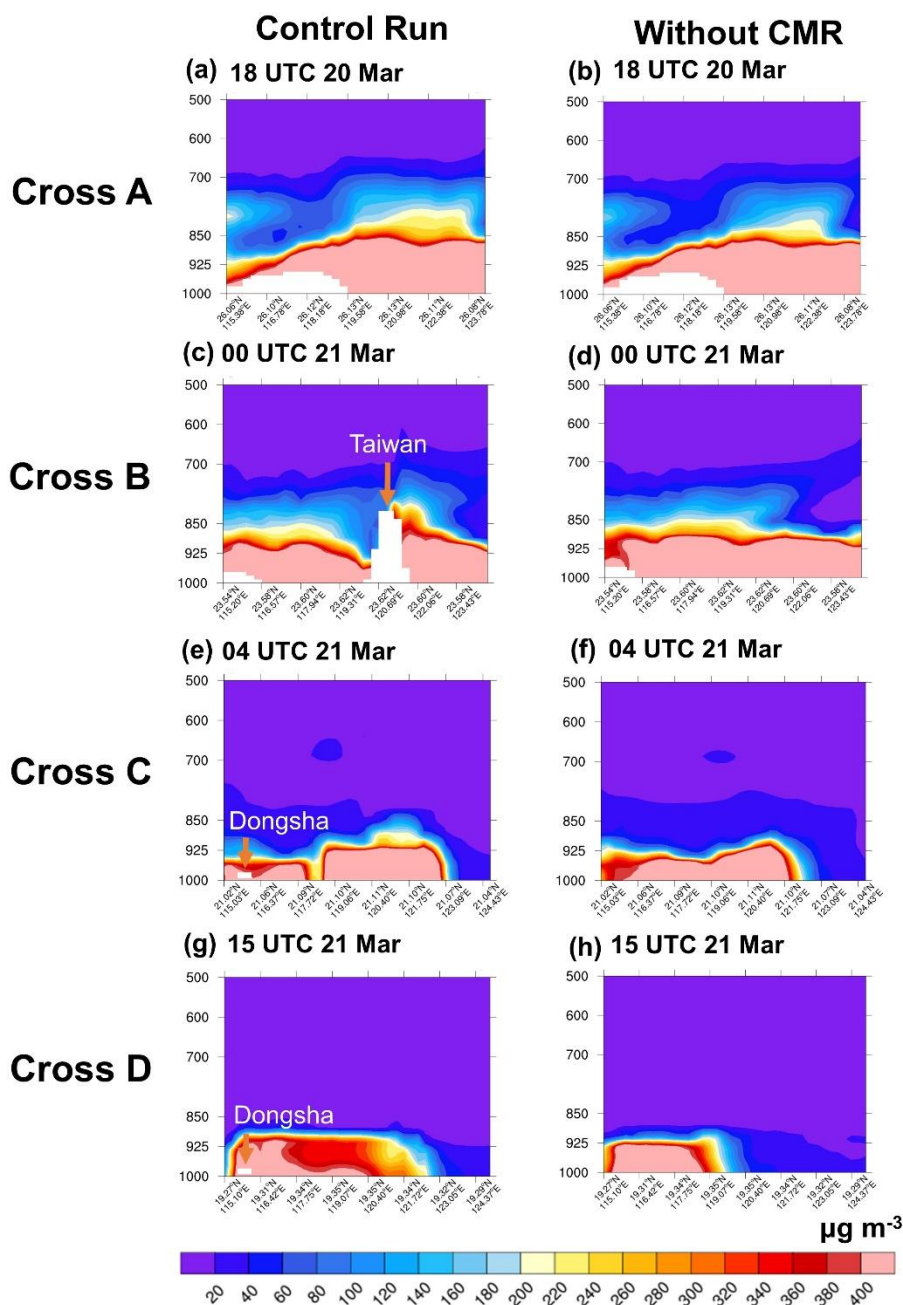
649

650 **Figure 5:** Spatial distribution of the simulated dust aerosol in the year 2010, during (a) 15 UTC 20
651 March, (b) 23 UTC 20 March, (c) 04 UTC 21 March, (d) 08 UTC 21 March, (e) 06 UTC 22 March and
652 (f) 12 UTC 22 March.

653

654

655



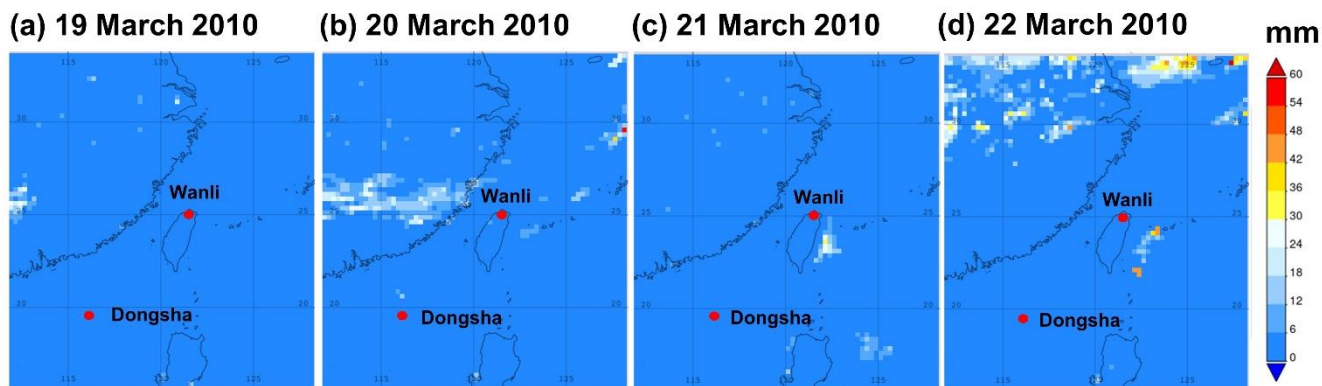
656

657 **Figure 6:** Vertical profile of dust aerosol for the CMAQ simulation of (a, c, e, g) control run and (b, d, f,
 658 h) without CMR at (a, b) 18 UTC 20 March, (c, d) 00 UTC 21 March, (e, f) 04 UTC 21 March and (g, h)
 659 15 UTC 21 March in the year of 2010.

660

661

662



663

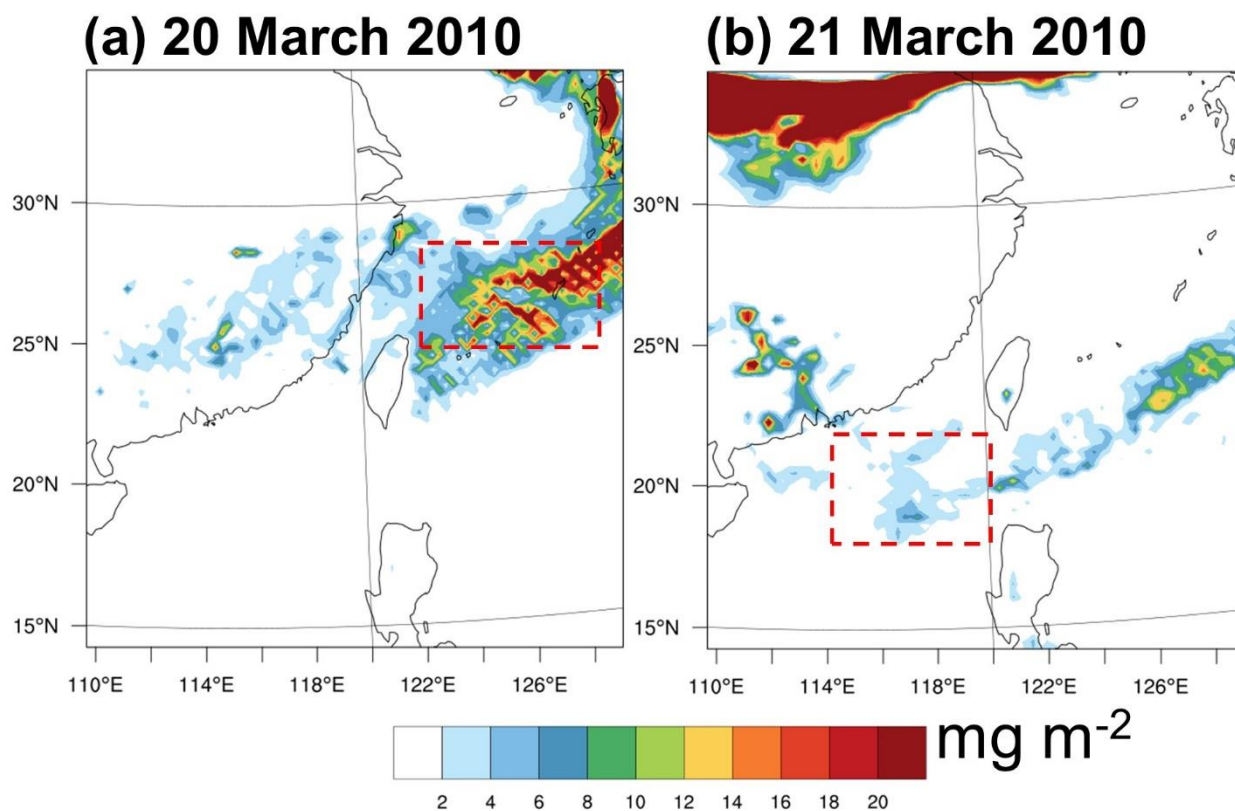
664

665

666

667

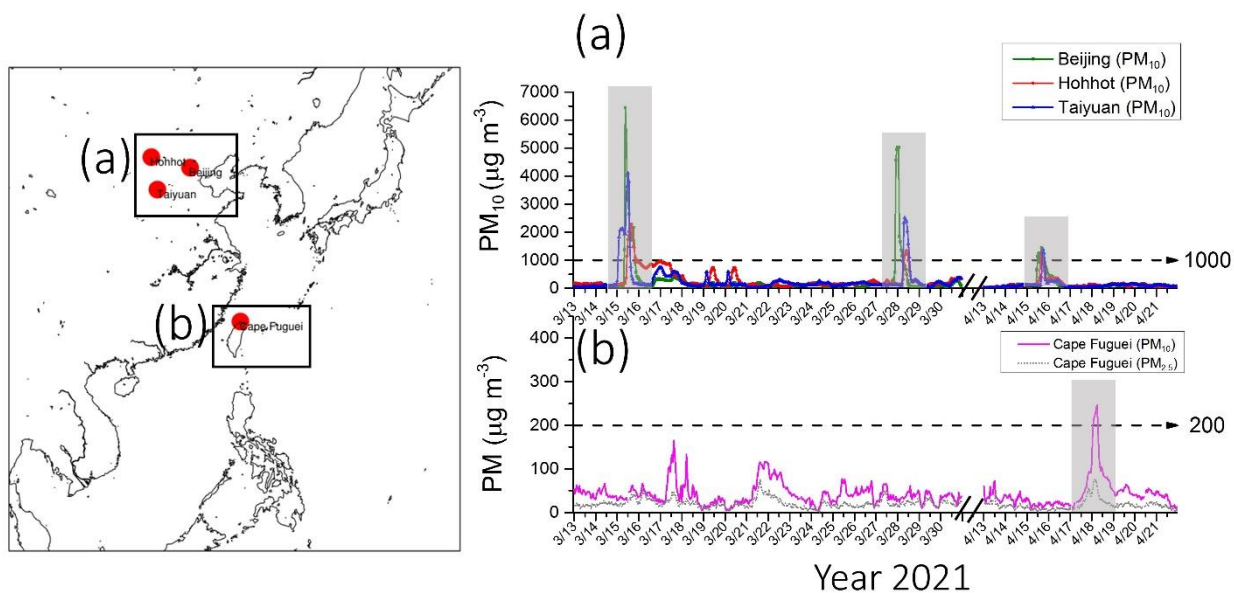
Figure 7: Daily mean merged precipitation data from the Global Precipitation Mission (GPM) satellite during 19-22 March 2010.



668

669

Figure 8: Spatial distribution of the wet deposition during (a) 20 March 2010 and (b) 21 March 2010.



670

671 **Figure 9:** Time series of the observed PM₁₀ concentrations over the source region including (a) Beijing,
672 Hohhot and Taiyuan; and the observed PM₁₀ and PM_{2.5} at (b) Cape Fuguei during the spring 2021.

673

674

675

676

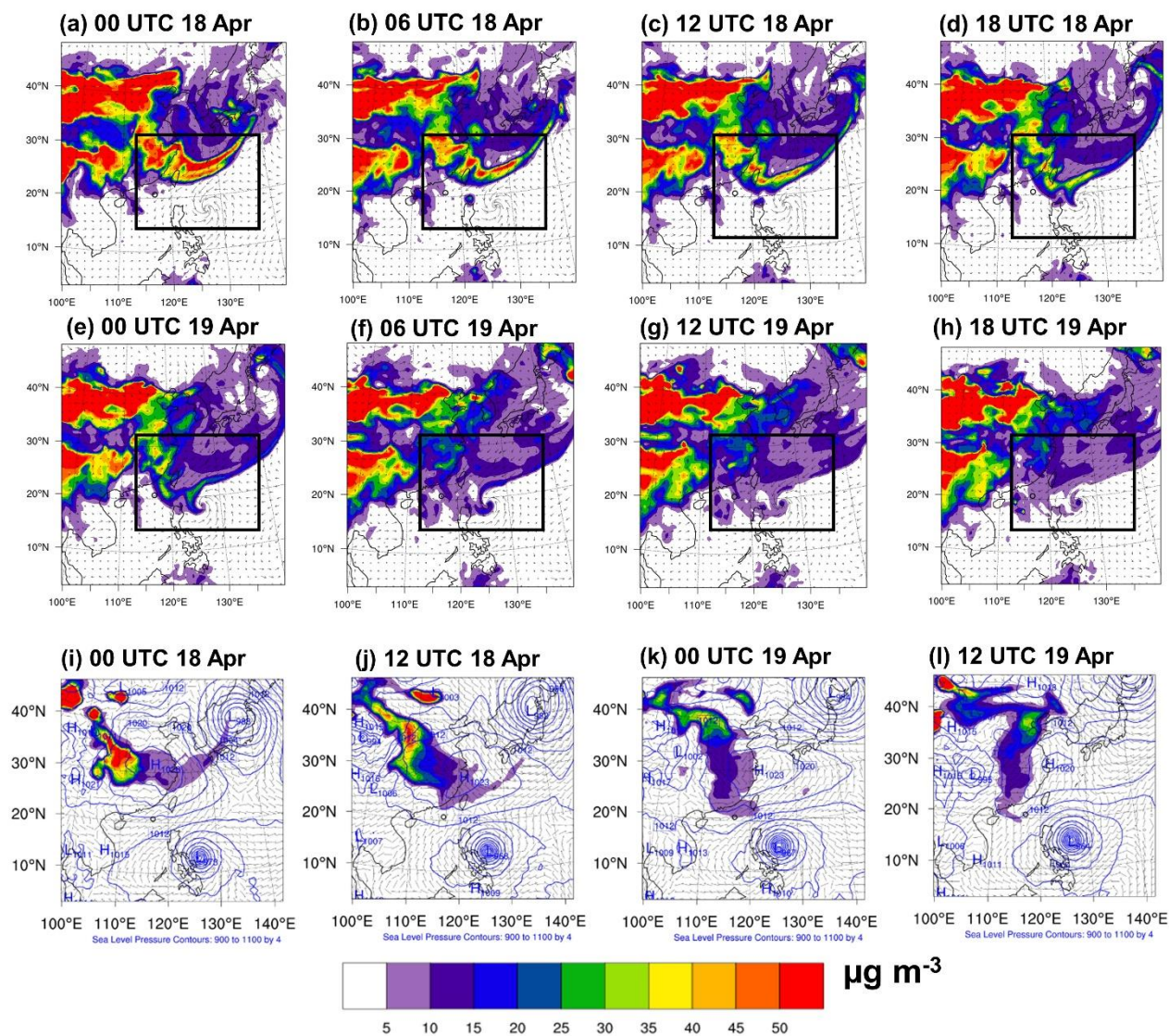
677

678

679

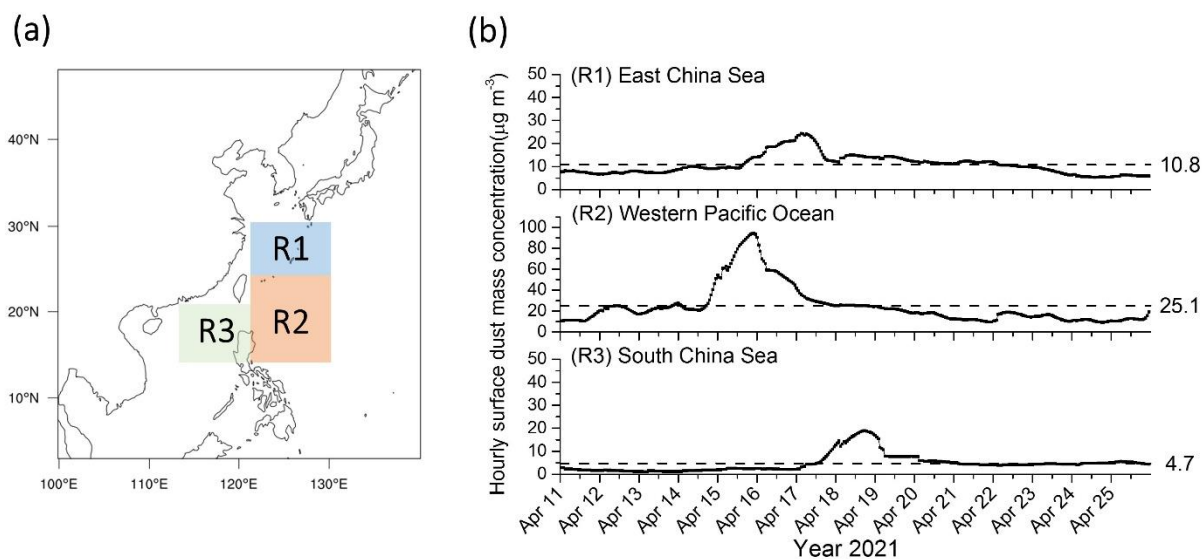


680



681
682
683
684
685
686
687
688
689
690
691
692

Figure 10: Spatial distribution of the MERRA-2 surface dust mass concentrations over the western North Pacific Ocean (shown in black rectangular box) during (a) 00 UTC 18 April, (b) 06 UTC 18 April, (c) 12 UTC 18 April, (d) 18 UTC 18 April, (e) 00 UTC 19 April, (f) 06 UTC 19 April, (g) 12 UTC 19 April and (h) 18 UTC 19 April 2021. The CMAQ surface dust mass concentrations during (i) 00 UTC 18 April, (j) 12 UTC 18 April, (k) 00 UTC 19 April and (l) 12 UTC 19 April 2021.



693

694 **Figure 11:** MERRA-2 hourly averaged dust mass concentrations over (a) R1: East China Sea, R2:
695 Western Pacific Ocean and R3: South China Sea, during (b) 11-25 April 2021. Black dash line indicates
696 the mean of dust mass concentration.

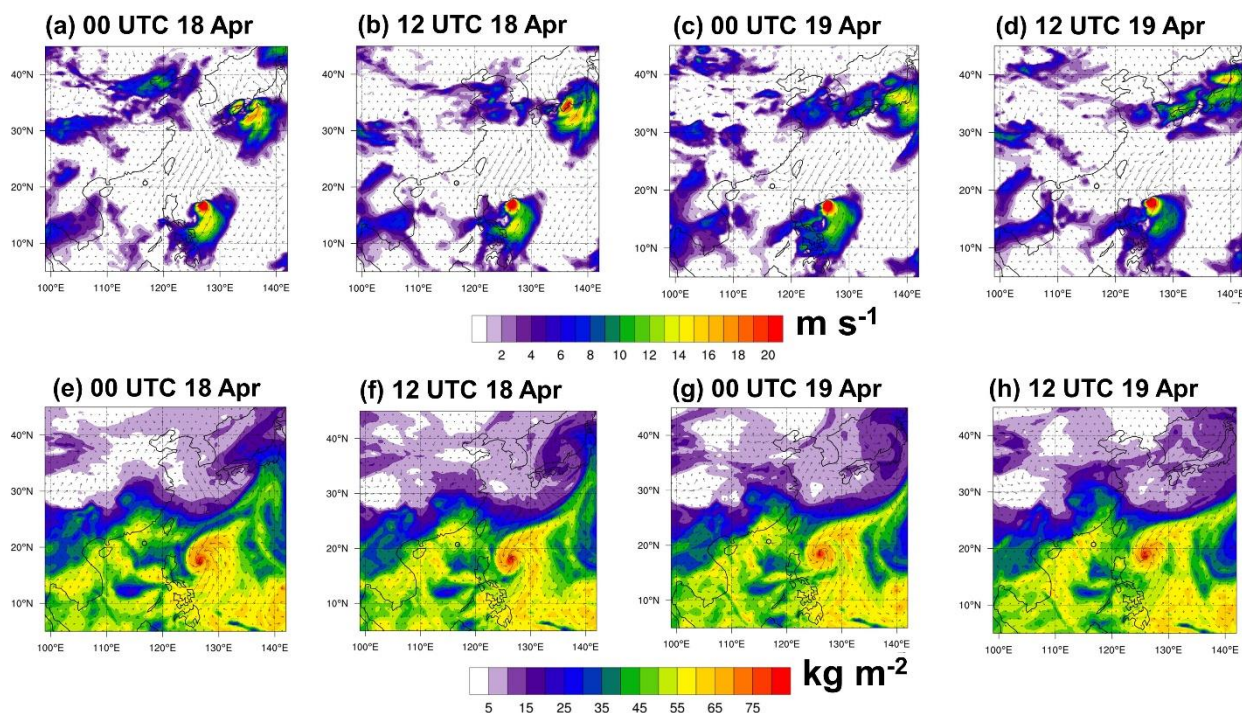
697

698

699

700

701



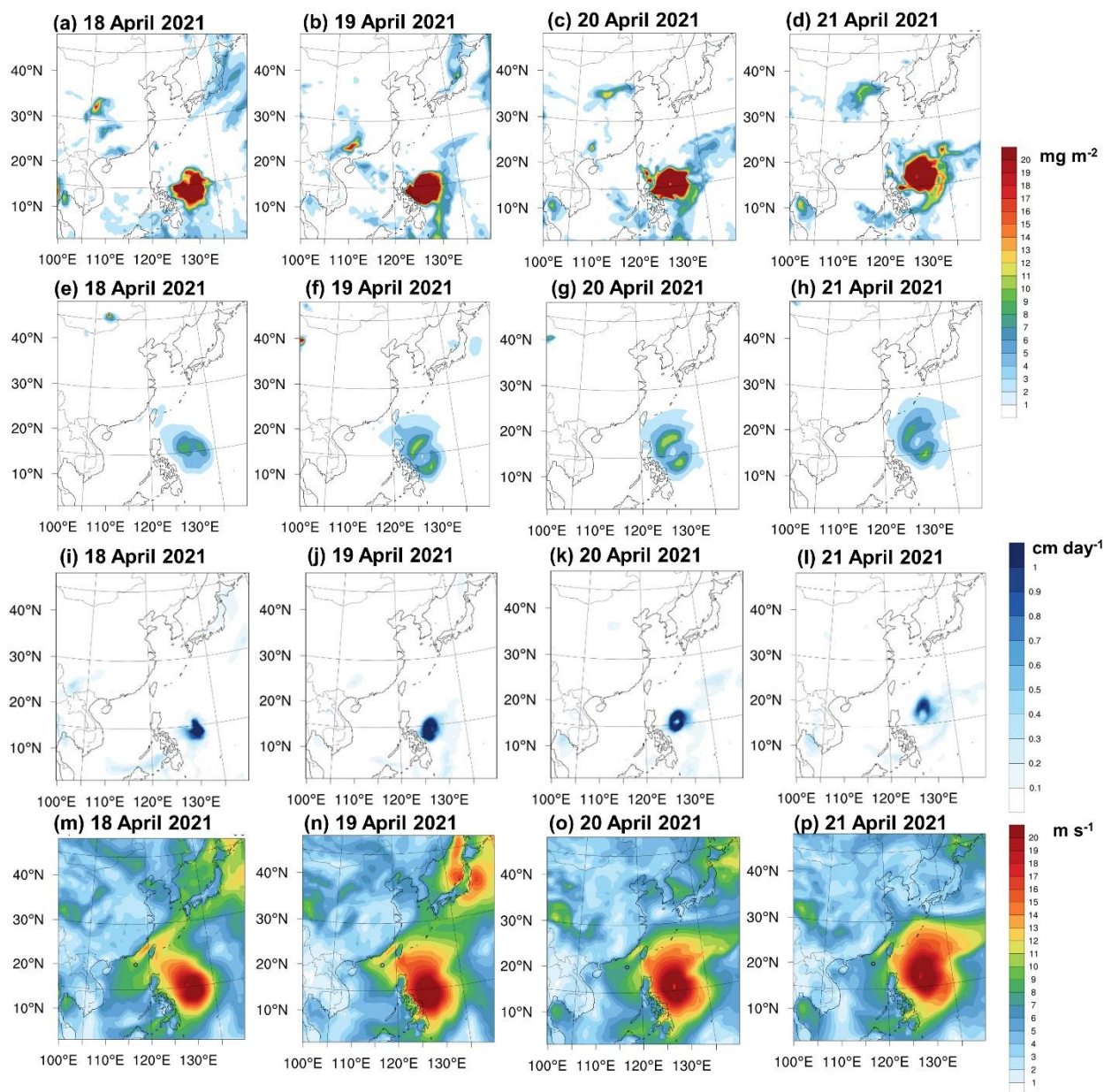
702

703 **Figure 12:** Spatial distribution of the MERRA-2 (a-d) wind speed and (e-h) total precipitation water
704 vapour during (a, e) 00 UTC 18 April, (b, f) 12 UTC 19 April, (c, g) 00 UTC 19 April and (d, h) 12
705 UTC 19 April 2021.

706

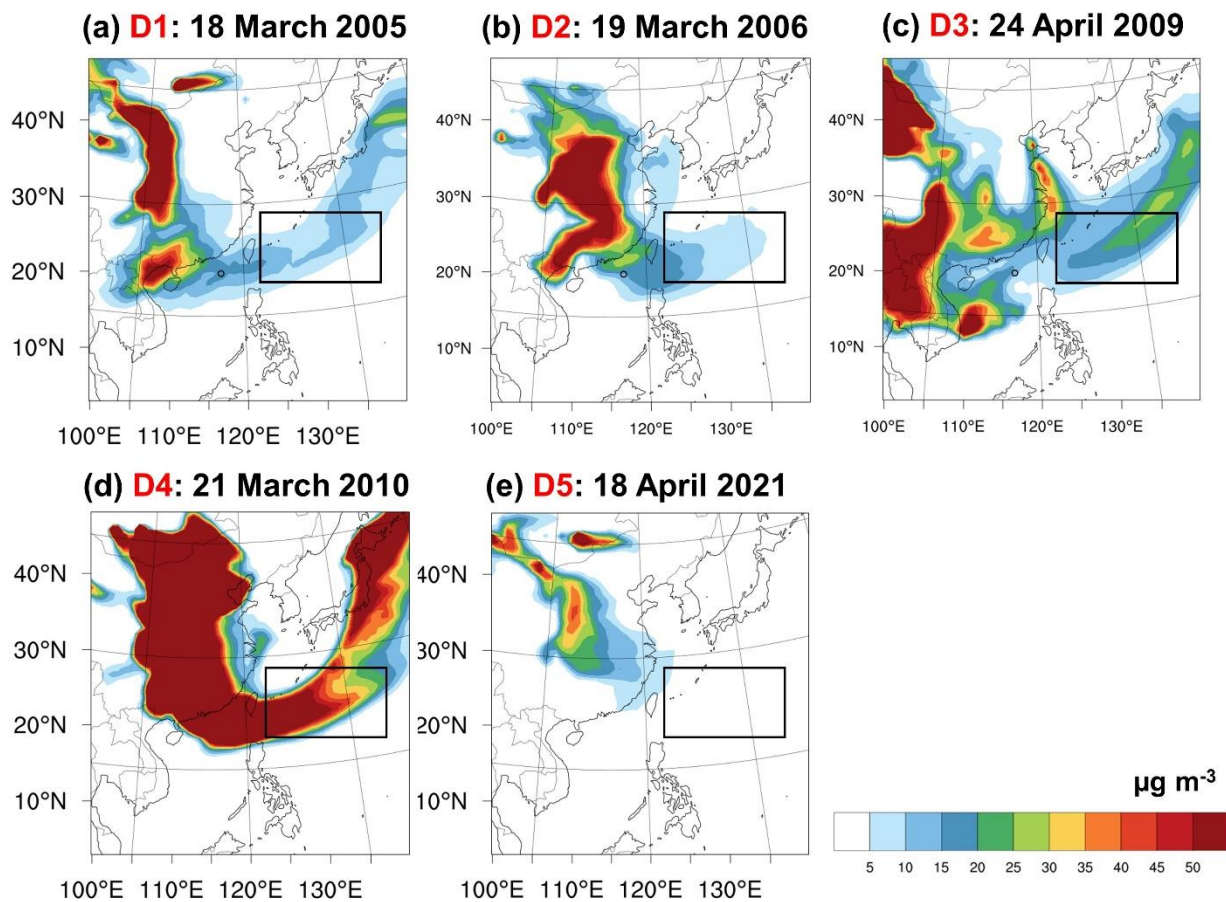
707

708



709

710 **Figure 13:** Spatial distribution of the (a-d) wet deposition, (e-h) dry deposition, (i-l) average daily
 711 precipitation and (m-p) daily mean wind speed during (a, e, i, m) 18 April, (b, f, j, n) 19 April, (c, g, k, o)
 712 20 April and (d, h, i, p) 21 April 2021.



713

714 **Figure 14:** Daily mean surface dust mass concentrations for (a) D1: 18 March 2005, (b) D2: 19 March

715 2006, (c) D3: 24 April 2009, (d) D4: 21 March 2010 and (e) D5: 18 March 2021.